Article

Ocean Dynamics Observed by VIIRS Day/Night Band Satellite Observations

Wei Shi [1,2,*] and Menghua Wang [1]

[1]National Oceanic and Atmospheric Administration, National Environmental Satellite, Data, and Information Service, Center for Satellite Applications and Research, E/RA3, 5830 University Research Ct., College Park, MD 20740, USA; Menghua.Wang@noaa.gov

[2]Cooperative Institute for Research in the Atmosphere at Colorado State University, Fort Collins, Colorado, USA.

*Correspondence: wei.1.shi@noaa.gov; Tel.: +1-301-683-3323; Fax: +1-301-683-3301

Abstract: Three cases of Day/Night Band (DNB) observations of the Visible Infrared Imaging Radiometer Suite (VIIRS) onboard the Suomi National Polar-orbiting Partnership (SNPP) are explored for applications to assess the ocean environment and monitor ocean dynamics. An approach to use the ratio between the target radiance and the reference radiance was developed in order to better assess the ocean diurnal and short-term environmental changes with VIIRS DNB observations. In the La Plata River Estuary, the sediment fronts showed 20–25 km diurnal inshore-offshore movements on 13 March 2017. In the waters off the Argentina coast in the South Atlantic, VIIRS DNB measurements provided both daytime and nighttime observations and monitoring of the algal bloom development and migration between 24–26 March 2016. This algal bloom generally kept the same spatial patterns, but moved nearly 20 km eastward in the three-day period. In the Yangtze River Estuary and Hangzhou Bay region in China's east coast, VIIRS DNB observations also revealed complicated coastal dynamic changes between 12–14 April 2017. Even though there are still some challenges and limitations for monitoring the ocean environment with VIIRS DNB observations, this study shows that satellite DNB observations can provide additional data sources for ocean observations, especially observations during the nighttime.

Keywords: VIIRS; DNB observation; ocean dynamics; satellite remote sensing; ocean color; nocturnal study

1. Introduction

The Visible Infrared Imaging Radiometer Suite (VIIRS) is one of the key instruments onboard the Suomi National Polar-orbiting Partnership (SNPP) satellite launched on 28 October 2011. In addition to its operational uses, an important research goal of VIIRS is to provide data continuity for the Moderate Resolution Imaging Spectroradiometer (MODIS) long-term measurements of Earth's atmosphere, land, and ocean properties [1]. VIIRS has spectral bands similar to MODIS, with 22 spectral bands covering a range of 0.410–12.013 μm. VIIRS measurements include 14 reflective solar bands (RSBs), 7 thermal emissive bands (TEBs), and a panchromatic Day/Night Band (DNB). As a new and additional band to the conventional RSBs and TEBs, the DNB provides visible and near-infrared (NIR) spectral imagery of Earth under a wide range of illumination conditions from full sunlight to night illumination (e.g., moonlight) or emission (e.g., from terrestrial sources). The DNB measures the reflectance from Earth and atmosphere in the wavelengths from 500 to 900 nm at a 742 m spatial resolution. The DNB measurement dynamic range is from 3×10^{-9} to 2×10^{-2} W cm^{-2} sr^{-1}. The VIIRS DNB radiance is well-calibrated on orbit, performs suitably, and meets the sensor specifications [2-5].

SNPP-VIIRS DNB observations introduce a unique frontier of nighttime environmental sensing capabilities [6, 7] to complement traditional infrared-based observations. Given its ability to detect both natural and artificial light sources, DNB nighttime low-light observations are expanding our sphere of knowledge for the natural sciences and social sciences [7]. Using VIIRS DNB measurements, Earth's cryosphere, hydrosphere, and lithosphere can be further characterized [7], e.g., detecting diffused light at the cloud top with nearby lightning flashes [8], retrieving low-level circulation of tropical cyclones via moonlight reflectance [7, 9], detecting and assessing marine bioluminescence and biomass burning [10, 11], and deriving nighttime air quality information [12]. In addition, DNB observations are useful for societal benefits with various applications such as identifying ship track and boat locations [13, 14], measuring and monitoring light power and electricity supply reliability [2, 15, 16], assessing and evaluating urban development and population dynamics [17, 18], and estimation of the improvement and progress of global and regional economics [19, 20].

Satellite ocean color remote sensing has long been used to study physical, optical, biological, and biogeochemical processes in the global ocean. A variety of satellite ocean color products such as normalized water-leaving radiance spectra [21, 22], chlorophyll-a (Chl-a) concentration [23], diffuse attenuation coefficient at 490 nm $K_d(490)$ [24, 25], total suspended matter (TSM) concentration [26-28], inherent optical properties (IOPs) [29, 30], and ocean primary productivity [28, 31, 32] have been produced to monitor and evaluate the ocean dynamics and variability for the global open ocean and coastal waters. Traditionally, all of these satellite ocean color products are derived during the daytime, and there is no information about ocean property changes at night. In this study, we examine how ocean observations from the VIIRS DNB band can be used to assess and evaluate a variety of ocean physical and biological variabilities such as sediment front movement, phytoplankton bloom migration, and complex estuary dynamics. Thus, the VIIRS DNB measurements provide the capability to continuously monitor and assess ocean dynamics during both daytime and nighttime. In this study, an approach to use the DNB radiance ratio was developed in order to better assess the ocean diurnal and short-term environmental changes with VIIRS DNB observations. Three cases were explored to evaluate the sediment front movement, phytoplankton bloom migration, and complex estuary dynamics with VIIRS observations.

2. Data and Methods

VIIRS DNB Sensor Data Records (SDR) were obtained from the NOAA Comprehensive Large Array-DATA Stewardship System (CLASS). During the prelaunch phase of SNPP, the DNB relative spectral response (RSR) was carefully characterized in a laboratory environment. The Horizontal Sample Interval (HSI) is 742 m (±5%) with a geolocation uncertainty of 400 m at nadir. Three sets of low gain set (LGS), mid-gain set (MGS), and high gain set (HGS) were applied selectively on DNB measurements due to the wide ranges of the radiance measurement for the daytime and nighttime scenes. Stray light contamination in the DNB measurements was also removed during post-processing. After radiometric calibration, the signal-noise-ratio (SNR) was larger than 9 across the entire scan at DNB minimum radiance L_{min} of 3×10^{-9} W cm^{-2} sr^{-1}. Note that the VIIRS DNB radiance is reported as a band-integrated total radiance.

Well-calibrated VIIRS DNB measurements make it possible to characterize ocean dynamics features under lunar illumination conditions even though the radiometric signals from the ocean are significantly weaker than from the other targets such as the land and atmosphere. In this study, the top-of-atmosphere (TOA) radiance measurements from VIIRS DNR are used to characterize diurnal changes of the ocean's physical, biological, and biogeochemical features. However, DNB TOA radiance for assessing ocean feature dynamics is not very effective due to the following reasons: (1) the DNB TOA radiance signals are typically weak and noisy during the nighttime, (2) the DNB radiance during the daytime is several orders

higher than those from the nighttime, and (3) the downwelling lunar illuminance at the ocean surface can be highly variable due to the phases of the lunar cycle and different atmospheric conditions.

In this study, a radiance ratio approach is developed to better characterize and possibly quantify the ocean features observed by VIIRS DNB. Specifically, a median value of DNB radiance in a target region is selected as the background reference radiance, and then this reference DNB radiance is used to normalize the DNB observations by calculating the DNB radiance ratio for each VIIRS pixel, i.e.,

$$R(\mathrm{DNB}) = L(\mathrm{DNB})/L_{\mathrm{ref}}(\mathrm{DNB}), \quad (1)$$

where L(DNB) and L_{ref}(DNB) are the VIIRS-measured DNB radiance and the median DNB radiance over the ocean in a targeted region, respectively.

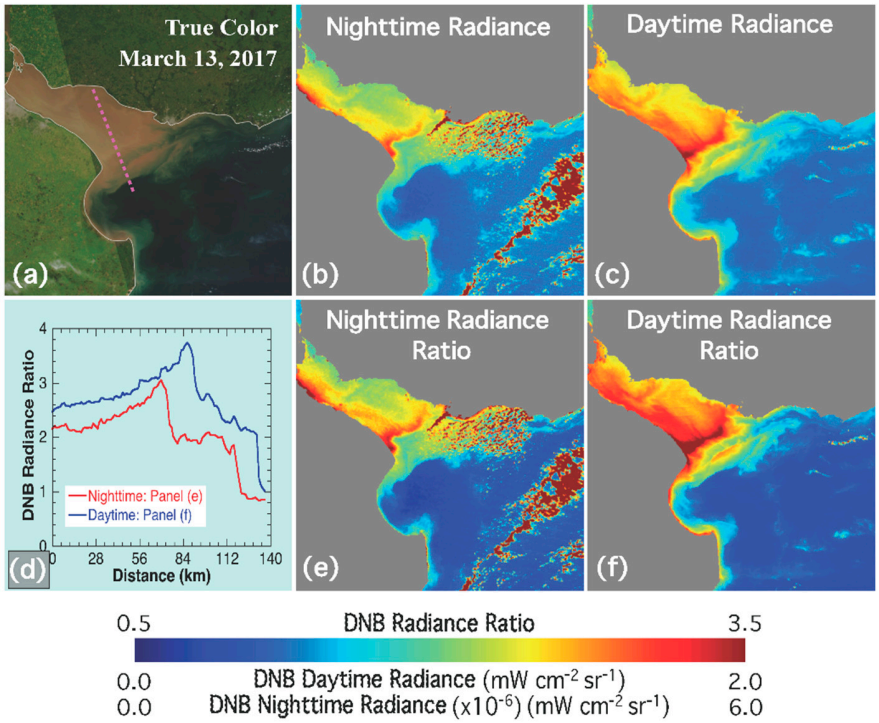

Figure 1. VIIRS-observed diurnal change of the La Plata River Estuary for (a) RSB daytime true color image at 16:47 UTC on 13 March 2017, (b) DNB nighttime TOA radiance at 04:27 UTC on 13 March 2017, (c) DNB daytime TOA radiance at 16:47 UTC on 13 March 2017, (d) DNB radiance ratio R along the transect line indicated in Fig. 1a, (e) DNB nighttime TOA radiance ratio at 04:27 UTC on 13 March 2017, and (f) DNB daytime TOA radiance ratio at 16:47 UTC on 13 March 2017.

In this study, the DNB scenes over the target area were first visually examined to make sure they were relatively clear-sky scenes with only sporadic isolated cloud coverage. DNB measurements over cloud-contaminated pixels are significantly higher (more than 10 times) than the non-cloud ocean pixels. The domain size for the L_{ref}(DNB) computation is generally a couple of times larger than the interest target area. It is also noted that the median value instead of the mean value of L(DNB) is used to compute the L_{ref}(DNB). Thus, this approach can avoid the overweight of the cloud-contaminated pixels when L_{ref}(DNB) is calculated, i.e., outliers are generally filtered out. It is found that the L_{ref}(DNB) change is small and less sensitive to the domain size when the domain size becomes even larger. In addition, L_{ref}(DNB) is also stable and less sensitive to the scarce cloud-contamination in the domain in the statistical calculation.

With the DNB radiance ratio R(DNB), the ocean features as observed by VIIRS DNB for daytime and nighttime, as well as for different lunar phases become comparable. Thus, the images of the DNB radiance ratio R(DNB) can be easily used to study the diurnal ocean dynamics. In this study, we show three cases that demonstrate the VIIRS DNB observations that can be used to study and monitor (1) the ocean's sediment fronts, (2) development and migration of the phytoplankton algal blooms, and (3) coastal and estuarine ocean dynamics.

3. Results

3.1. Diurnal variation of sediment fronts

La Plata River Estuary located between Argentina and Uruguay, and near Buenos Aires is one of the most turbid water regions in the world [33]. Figure 1 shows the diurnal variation of the sediment fronts at the La Plata River Estuary on 13 March 2017 around the night of a full Moon. Figure 1a shows the daytime true color image as collected by the VIIRS RSBs at 16:47 UTC. It clearly shows the sediment fronts between the La Plata River Estuary and the open ocean.

Figure 1b shows the DNB radiance measurements during the nighttime on 13 March 2017 at 04:27 UTC, and Fig. 1c is the DNB daytime radiance from the same time (16:47 UTC) as the RSB true color image in Fig. 1a. Two sediment fronts are shown on both nighttime and daytime DNB observations with enhanced sediment concentrations for the inner front and the clear boundary between estuary waters and open ocean for the outer front. It is also noted that DNB radiance in the daytime is six orders higher than those in the nighttime.

Figures 1e and 1f further characterize the diurnal changes of the two sediment fronts. Notable expansion of the estuary sediment water can be found progressing from the nighttime observation to the daytime observation, about 12 hours later. Both fronts were located further offshore during the daytime. Note that DNB radiance ratios in the open offshore region for both nighttime (Fig. 1e) and daytime (Fig. 1f) are similar. Since the offshore ocean is generally stable in a 12-hour period, the similar DNB radiance ratio values provide evidence that the atmospheric conditions (i.e., atmospheric properties) are stable. Thus, the DNB radiance ratios may be used to evaluate ocean changes quantitatively. The pronounced DNB radiance ratio during the daytime (Fig. 1f) also suggests that the overall sediment concentration in the La Plata River Estuary is much higher than that during the nighttime. The quantitative evaluation of the DNB radiance ratio (Fig. 1d) shows the locations of the two sediment fronts and the broad enhancement of the DNB radiance ratio during the daytime in comparison with that during the nighttime. In the period between the nighttime and daytime observations, the inner front moved offshore about 25 km, while the outer front moved offshore about 20 km along the transect crossing the two sediment fronts. These observations are important to assess the coastal and estuarial environment and ecosystem, as well as to improve the ocean physical and biogeochemical modeling.

Preprints (www.preprints.org) | NOT PEER-REVIEWED | Posted: 13 December 2017 doi:10.20944/preprints201712.0078.v1

Peer-reviewed version available at Remote Sens. 2018, 10, 76; doi:10.3390/rs10010076

3.2. Migration of algal bloom off the Argentina coast

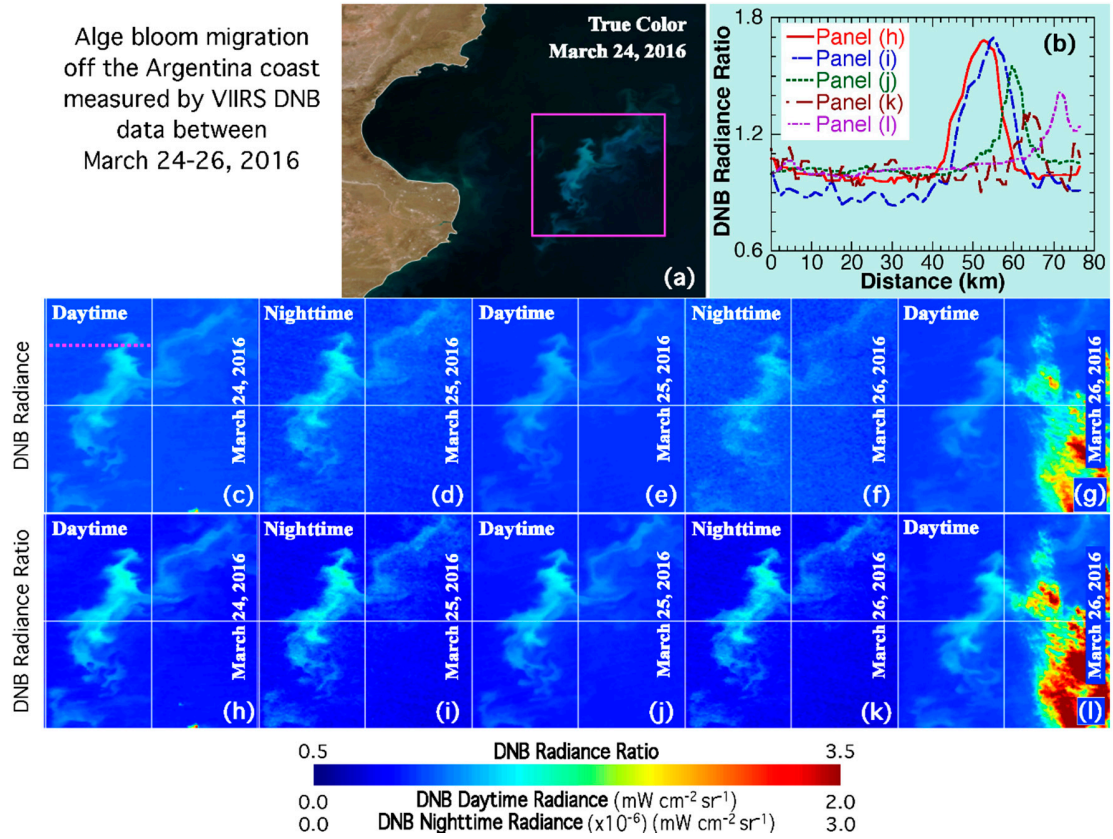

Figure 2. VIIRS-observed algal bloom off the Argentina coast in the South Atlantic for (a) RSB daytime true color image at 17:19 UTC on 24 March 2016 with the marked box region for further analysis using VIIRS DNB observations, (b) DNB radiance ratio *R* along the transect line indicated in Fig. 2c with different daytime and nighttime observations, (c–g) DNB TOA radiance at 17:19 UTC on 24 March 2016, 04:48 UTC on 25 March 2016, 18:44 UTC on 25 March 2016, 04:30 UTC on 26 March 2016, 18:27 UTC on 26 March 2016, respectively, and (h–l) DNB TOA radiance ratio at 17:19 UTC on 24 March 2016, 04:48 UTC on 25 March 2016, 18:44 UTC on 25 March 2016, 04:30 UTC on 26 March 2016, and 18:27 UTC on 26 March 2016, respectively.

Algal bloom is a common biological feature found off the Argentinian coast of the South Atlantic. Even though satellite ocean color sensors like MODIS and VIIRS can provide observations of the biological variability, clear-sky observation requirements in the daytime can significantly limit the capability of the satellite ocean color sensor to monitor the ocean biological variation. Figure 2 shows the evolving structure of an algal bloom between 24–26 March 2016 using VIIRS DNB observations. Figure 2a shows the true color image of this algal bloom on 24 March with the daytime true color image from VIIRS RSB bands. Figures 2c–2g are the chronological radiance observations captured by the VIIRS DNB band for the daytime on 24 March (Fig. 2c), nighttime on 25 March (Fig. 2d), daytime on 25 March (Fig. 2e), nighttime on 26 March (Fig. 2f), and daytime on 26 March (Fig. 2g). Even though DNB radiance during the nighttime were noisier than the daytime values due to low signals in the nighttime, the nighttime DNB radiance still clearly shows the location and extent of the algal bloom.

Figures 2h–2l show the corresponding DNB radiance ratio images calculated between 24–26 March 2016. Locations and the coverage extents of this algal bloom are better presented with the DNB radiance ratio images in comparison with the DNB radiance images. In the three-day period, this algal bloom

generally maintained a similar spatial pattern. However, the continuous DNB observations from both the DNB radiance (Figs. 2c–2g) and DNB radiance ratio (Figs. 2h–2l) show how this algal bloom patch moved to the east and southeast direction.

DNB radiance ratio values along the transect line indicated in Fig. 2c show the migration of this algal bloom over three days. Figure 2b further describes the migration of the algal bloom with the DNB radiance ratio along the transect line. In the daytime of 24 March, the peak of the DNB radiance ratio was located at ~52 km eastward at this transect. In the next two days, it gradually moved further eastward with locations at ~55 km in the nighttime of 25 March (Fig. 2d), ~59 km in the daytime of 25 March, ~64 km in the nighttime of 26 March, and ~70 km in the daytime of 27 March. It is also noted that DNB radiances were generally flat and consistent with each other for the five VIIRS DNB observations for the non-algae ocean at the range of 0–40 km from the transect. This suggests that the DNB radiance ratio approach can largely filter out the background signals at different observation times, and make the daytime and nighttime DNB observations comparable in order to monitor the migration and development of the algal bloom.

3.3. Coastal dynamics along the China's east coast

In a complicated coastal region such as China's east coast, coastal dynamics is driven by multiple forces such as tides [34, 35], river flow, current [36], and winds [37]. In order to better characterize and monitor these coastal environments, nighttime observations from the VIIRS DNB band can provide valuable complementary information about the coastal ocean dynamics.

Figure 3 shows coastal ocean dynamics between 12–14 April 2017 from VIIRS DNB observations in the Yangtze River Estuary and Hangzhou Bay region along China's east coast. This coastal region is comprised of various water masses as shown in the true color image (Fig. 3a). The TOA DNB radiance can also provide a qualitative assessment of coastal environmental changes. Comparing the nighttime and daytime DNB radiances (Figs. 3c–3e), the plume from the coastal turbid waters is seen to extend further offshore in the daytime DNB radiance measurement on 14 April 2017 (Fig. 3f). Nighttime DNB observations (Figs. 3c and 3e) provide the diurnal changes of the coastal sediment patches and swirls in reasonably high quality images. This is especially true at the mouth of the south and north channels of the Yangtze River Estuary where the ocean geophysical and biological features are complicated and highly dynamic.

Figures 3g–3j provide the quasi-quantitative assessment of the coastal dynamics of the Yangtze River Estuary using TOA DNB radiance ratio for this period. In the clear open ocean, the TOA DNB radiance ratios are generally consistent in the four images, further suggesting that the DNB radiance ratio approach can largely remove the difference caused by the day-night and lunar phase issues from the DNB observations. Thus, it can be used to compare different DNB observations over the ocean environment. On the other hand, enhanced TOA DNB radiance ratios for the nighttime observation at 17:59 UTC on 13 April 2017 (Fig. 3i) and the daytime observation at 05:16 UTC on 14 April 2017 (Fig. 3j) in the Hangzhou Bay suggest that the TSM concentration in the Hangzhou Bay increased with time in the period between 12–14 April 2017. A similar TSM concentration trend can also be found in the Yangtze River Estuary.

Figure 3b further analyzes the coastal dynamics along the cross-shelf transect off the northern branch of the Yangtze River Estuary as shown in Fig. 3a with the DNB radiance ratio. Significant diurnal variations occurred along this transect. Elevated DNB radiance ratios are evident in Figs. 3i and 3j, 30 km offshore. Specifically, a significant drop of the DNB radiance ratio at ~30–40 km range in Fig. 3i suggests an enhanced sediment front in the nighttime observation on 13 April 2017. At the location of ~70 km offshore, a remarkable DNB radiance ratio in Fig. 3j indicates that TSM concentrations at this location at 05:16 UTC on 14 April 2017 were much higher than those from the other three DNB observations. In the distance range beyond ~100 km offshore, the stable and consistent DNB radiance ratio for all four DNB radiance ratio images further imply that the ocean was less dynamic than the coastal inshore waters. It is also noted that enhanced radiance and radiance ratios existed near the coast, and over the marine structure during the nighttime DNB observations in Fig. 3c/3g and Fig. 3e/3i. These are attributed to the diffuse glow from city lights. The sporadic isolated cirrus cloud features can also be found in daytime imagery in Figs 3f and 3j. These small features can be easily identified in the image, but can have minor effects on the computation of the typical $L_{ref}(DNB)$.

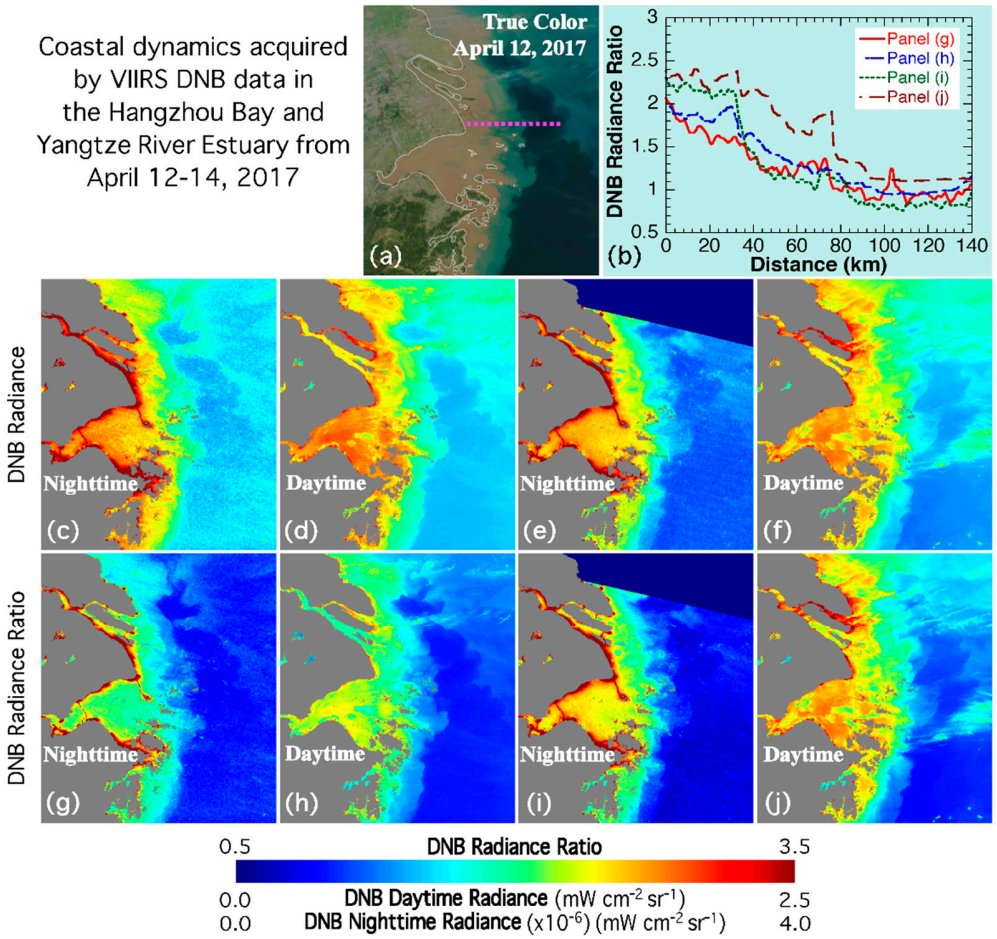

Figure 3. Coastal dynamics in the Hangzhou Bay and Yangtze River Estuary along China's east coast between 12–14 April 2017 for (a) RSB daytime true color image on 13 April 2017, (b) DNB radiance ratio *R* along the transect line indicated in Fig. 3a with different daytime and nighttime observations, (c–f) DNB TOA radiance at 18:16 UTC on 12 April 2017, 05:33 UTC on 13 April 2017, 17:59 UTC on 13 April 2017, 05:16 UTC on 14 April 2017, respectively, and (g–j) DNB TOA radiance ratio at 18:16 UTC on 12 April 2017, 05:33 UTC on 13 April 2017, 17:59 UTC on 13 April 2017, and 05:16 UTC on 14 April 2017, respectively.

4. Discussion and Summary

In this study, we used three cases to illustrate how VIIRS DNB observations can be used to characterize the ocean front of suspended sediment, monitor the motion of an algal bloom, and visualize coastal ocean dynamics. In addition to the TOA radiance measured by VIIRS DNB band, a new approach using the DNB radiance ratio based on the normalization by the reference scene radiance is proposed. It is noted that the L_{ref}(DNB) is generally less sensitive to the sporadic cloud coverage of the target region. As an example, L_{ref}(DNB) for the nighttime DNB observations corresponding to Fig. 1b is 1.50×10^{-6} mW $cm^{-2}sr^{-1}$. L_{ref}(DNB) value will become 1.46×10^{-6} mW $cm^{-2}sr^{-1}$ if a filter with 5× L_{ref}(DNB) as threshold is applied to filter out the cloud pixels. The impact on the radiance ratio image is trivial and negligible. Similar situations are also true for other two cases. The ratio makes the daytime and nighttime DNB observation comparable for an improved continuous assessing and monitoring of ocean dynamics. Monitoring sediment front movements, algal bloom development and migration, and dynamics of coastal and estuarine waters benefit from the dual daytime and nighttime VIIRS DNB observations.

By extending this capability to the night, these VIIRS DNB data provide a unique observation capability to study diurnal changes of the ocean environment. Even though many limitations and challenges for DNB observations over the ocean still exist, this study demonstrates one more example of how the DNB observation has the potential to provide new capabilities, tools, and data resources for satellite ocean studies, especially during the nighttime, in addition to the already well-known applications of the satellite DNB observations.

There are other approaches such as Near Constant Contrast (NCC) [38, 39] to produce contrast imagery for comparing daytime and nighttime observations. However, the method used in this study has several advantages for the DNB observations over the ocean. From atmospheric correction point of view, using a typical L_{ref}(DNB) in the nearby region and computing the L(DNB)/L_{ref}(DNB) ratio can largely remove the effects of the atmosphere reflectance in the DNB observations since the pixel geometry (solar or lunar and sensor angles) and atmospheric condition are similar and ocean reflectance is weak. If the atmosphere conditions (i.e., atmosphere and aerosol properties) in the daytime and nighttime are the same, the daytime and nighttime radiance ratios are then coming from the ocean reflectance change. Thus, the DNB daytime and nighttime ratio images can be compared quantitatively.

There remain challenges, limitations and opportunities with regards to satellite DNB observations and applications to ocean environments. First, VIIRS DNB observations over the ocean depend on the magnitude of lunar illumination [40]. This determines that the best DNB observations for the ocean environment monitoring can only be available in the near full moon phase, i.e., full moon ±3 days. For the other lunar phases, the quality of DNB observations over the ocean degrades significantly due to the low lunar irradiance. It is also noted that moon glint can occur in DNB imagery, especially near the last quarter phase, posing an additional challenge. Second, even though a dynamic lunar irradiance model [41] has the potential to be applied to nighttime VIIRS DNB observations, it is still very challenging to quantitatively derive the ocean radiance contributions, i.e., normalized water-leaving radiances, from the DNB band due to the difficulty of accurate characterization of the lunar irradiance and the lack of an approach to conduct atmospheric correction. Essentially, this is because of very low signals measured by the satellite. Thus, the result shown in this paper is a good first step toward further studying the topic. Third, the DNB radiance ratio approach demonstrated in this study can be used for ocean dynamics analysis from different DNB observations. This might suggest that some possible ocean products such as TSM concentration can be derived from satellite DNB observations. However, more in situ data and a better characterization of the impacts of the atmospheric condition changes are still needed in order to develop the DNB ocean products like the satellite ocean color products in order to quantify the ocean changes for both the daytime and nighttime.

Acknowledgments: VIIRS DNB SDR data were obtained from NOAA CLASS (www.class.ngdc.noaa.gov). We thank three anonymous reviewers for their useful comments. The views, opinions, and findings contained in this paper are those of the authors and should not be construed as an official NOAA or U.S. Government position, policy, or decision.

References

1. Goldberg, M. D.; Kilcoyne, H.; Cikanek, H.; Mehta, A. Joint Polar Satellite System: The United States next generation civilian polar-orbiting environmental satellite system. *J Geophys Res-Atmos* **2013,** 118, (24), 13463-13475.
2. Cao, C. Y.; Bai, Y. Quantitative Analysis of VIIRS DNB Nightlight Point Source for Light Power Estimation and Stability Monitoring. *Remote Sens-Basel* **2014,** 6, (12), 11915-11935.
3. Cao, C. Y.; Xiong, J.; Blonski, S.; Liu, Q. H.; Uprety, S.; Shao, X.; Bai, Y.; Weng, F. Z. Suomi NPP VIIRS sensor data record verification, validation, and long-term performance monitoring. *J Geophys Res-Atmos* **2013,** 118, (20).
4. Liao, L. B.; Weiss, S.; Mills, S.; Hauss, B. Suomi NPP VIIRS day-night band on-orbit performance. *J Geophys Res-Atmos* **2013,** 118, (22), 12705-12718.
5. Sun, J. Q.; Wang, M. H. Optimized calibration methodology of VIIRS day-night band low-gain stage using a solar diffuser. *Appl Optics* **2017,** 56, (15), 4433-4442.
6. Miller, S. D.; Mills, S. P.; Elvidge, C. D.; Lindsey, D. T.; Lee, T. F.; Hawkins, J. D. Suomi satellite brings to light a unique frontier of nighttime environmental sensing capabilities. *P Natl Acad Sci USA* **2012,** 109, (39), 15706-15711.
7. Miller, S. D.; Straka, W.; Mills, S. P.; Elvidge, C. D.; Lee, T. F.; Solbrig, J.; Walther, A.; Heidinger, A. K.; Weiss, S. C. Illuminating the Capabilities of the Suomi National Polar-Orbiting Partnership (NPP) Visible Infrared Imaging Radiometer Suite (VIIRS) Day/Night Band. *Remote Sens-Basel* **2013,** 5, (12), 6717-6766.
8. Bankert, R. L.; Solbrig, J. E.; Lee, T. F.; Miller, S. D. Automated Lightning Flash Detection in Nighttime Visible Satellite Data. *Weather Forecast* **2011,** 26, (3), 399-408.
9. Pan, Y. F.; Liu, A. K.; He, S. Y.; Yang, J. S.; He, M. X. Comparison of Typhoon Locations over Ocean Surface Observed by Various Satellite Sensors. *Remote Sens-Basel* **2013,** 5, (7), 3172-3189.
10. Elvidge, C. D.; Baugh, K.; Zhizhin, M.; Hsu, F. C.; Ghosh, T. VIIRS night-time lights. *Int J Remote Sens* **2017,** 38, (21), 5860-5879.
11. Miller, S. D.; Haddock, S. H. D.; Elvidge, C. D.; Lee, T. F. Detection of a bioluminescent milky sea from space. *P Natl Acad Sci USA* **2005,** 102, (40), 14181-14184.
12. Zhao, X. R.; Shi, H. Q.; Yu, H.; Yang, P. L. Inversion of Nighttime PM2.5 Mass Concentration in Beijing Based on the VIIRS Day-Night Band. *Atmosphere-Basel* **2016,** 7, (10).
13. Elvidge, C. D.; Zhizhin, M.; Baugh, K.; Hsu, F. C. Automatic Boat Identification System for VIIRS Low Light Imaging Data. *Remote Sens-Basel* **2015,** 7, (3), 3020-3036.
14. Yamaguchi, T.; Asanuma, I.; Park, J. G.; Mackin, K. J.; Mittleman, J. Estimation of vessel traffic density from Suomi NPP VIIRS day/night band. *Oceans 2016 Mts/Ieee Monterey* **2016**.
15. Cole, T. A.; Wanik, D. W.; Molthan, A. L.; Roman, M. O.; Griffin, R. E. Synergistic Use of Nighttime Satellite Data, Electric Utility Infrastructure, and Ambient Population to Improve Power Outage Detections in Urban Areas. *Remote Sens-Basel* **2017,** 9, (3).
16. Mann, M. L.; Melaas, E. K.; Malik, A. Using VIIRS Day/Night Band to Measure Electricity Supply Reliability: Preliminary Results from Maharashtra, India. *Remote Sens-Basel* **2016,** 8, (9).
17. Shi, K. F.; Huang, C.; Yu, B. L.; Yin, B.; Huang, Y. X.; Wu, J. P. Evaluation of NPP-VIIRS night-time light composite data for extracting built-up urban areas. *Remote Sens Lett* **2014,** 5, (4), 358-366.
18. Tripathy, B. R.; Tiwari, V.; Pandey, V.; Elvidge, C. D.; Rawat, J. S.; Sharma, M. P.; Prawasi, R.; Kumar, P. Estimation of Urban Population Dynamics Using DMSP-OLS Night-Time Lights Time Series Sensors Data. *Ieee Sens J* **2017,** 17, (4), 1013-1020.
19. Li, X.; Xu, H. M.; Chen, X. L.; Li, C. Potential of NPP-VIIRS Nighttime Light Imagery for Modeling the Regional Economy of China. *Remote Sens-Basel* **2013,** 5, (6), 3057-3081.
20. Zhao, N. Z.; Hsu, F. C.; Cao, G. F.; Samson, E. L. Improving accuracy of economic estimations with VIIRS DNB image products. *Int J Remote Sens* **2017,** 38, (21), 5899-5918.

21. Gordon, H. R.; Wang, M. Retrieval of Water-Leaving Radiance and Aerosol Optical-Thickness over the Oceans with Seawifs - a Preliminary Algorithm. *Appl Optics* **1994,** 33, (3), 443-452.
22. IOCCG *Atmospheric Correction for Remotely-Sensed Ocean-Colour Products, M. Wang (Ed.)*. Dartmouth, Canada, 2010; p 77.
23. O'Reilly, J. E.; Maritorena, S.; Mitchell, B. G.; Siegel, D. A.; Carder, K. L.; Garver, S. A.; Kahru, M.; McClain, C. Ocean color chlorophyll algorithms for SeaWiFS. *J Geophys Res-Oceans* **1998,** 103, (C11), 24937-24953.
24. Lee, Z. P.; Darecki, M.; Carder, K. L.; Davis, C. O.; Stramski, D.; Rhea, W. J. Diffuse attenuation coefficient of downwelling irradiance: An evaluation of remote sensing methods. *J Geophys Res-Oceans* **2005,** 110, (C2).
25. Wang, M.; Son, S.; Harding, L. W. Retrieval of diffuse attenuation coefficient in the Chesapeake Bay and turbid ocean regions for satellite ocean color applications. *J Geophys Res-Oceans* **2009,** 114.
26. Miller, R. L.; McKee, B. A. Using MODIS Terra 250 m imagery to map concentrations of total suspended matter in coastal waters. *Remote Sens Environ* **2004,** 93, (1-2), 259-266.
27. Zhang, M.; Tang, J. W.; Dong, Q.; Song, Q. T.; Ding, J. Retrieval of total suspended matter concentration in the Yellow and East China Seas from MODIS imagery. *Remote Sens Environ* **2010,** 114, (2), 392-403.
28. Son, S.; Wang, M. Water properties in Chesapeake Bay from MODIS-Aqua measurements. *Remote Sens Environ* **2012,** 123, 163-174.
29. Garver, S. A.; Siegel, D. A. Inherent optical property inversion of ocean color spectra and its biogeochemical interpretation .1. Time series from the Sargasso Sea. *J Geophys Res-Oceans* **1997,** 102, (C8), 18607-18625.
30. Lee, Z. P.; Carder, K. L.; Arnone, R. A. Deriving inherent optical properties from water color: a multiband quasi-analytical algorithm for optically deep waters. *Appl Optics* **2002,** 41, (27), 5755-5772.
31. Behrenfeld, M. J.; O'Malley, R. T.; Siegel, D. A.; McClain, C. R.; Sarmiento, J. L.; Feldman, G. C.; Milligan, A. J.; Falkowski, P. G.; Letelier, R. M.; Boss, E. S. Climate-driven trends in contemporary ocean productivity. *Nature* **2006,** 444, (7120), 752-755.
32. Westberry, T.; Behrenfeld, M. J.; Siegel, D. A.; Boss, E. Carbon-based primary productivity modeling with vertically resolved photoacclimation. *Global Biogeochem Cy* **2008,** 22, (2).
33. Shi, W.; Wang, M. Satellite observations of the seasonal sediment plume in central East China Sea. *J Marine Syst* **2010,** 82, (4), 280-285.
34. Liu, X.; Wang, M. Analysis of ocean diurnal variations from the Korean Geostationary Ocean Color Imager measurements using the DINEOF method. *Estuar Coast Shelf S* **2016,** 180, 230-241.
35. Shi, W.; Wang, M.; Jiang, L. Spring-neap tidal effects on satellite ocean color observations in the Bohai Sea, Yellow Sea, and East China Sea. *J Geophys Res-Oceans* **2011,** 116.
36. Jiang, L.; Wang, M. Diurnal Currents in the Bohai Sea Derived From the Korean Geostationary Ocean Color Imager. *Ieee Transactions on Geoscience and Remote Sensing* **2017,** 55, (3), 1437-1450.
37. Shi, W.; Wang, M. Satellite views of the Bohai Sea, Yellow Sea, and East China Sea. *Prog Oceanogr* **2012,** 104, 30-45.
38. Liang, C. K.; Mills, S.; Hauss, B. I.; Miller, S. D. Improved VIIRS Day/Night Band Imagery With Near-Constant Contrast. *Ieee Transactions on Geoscience and Remote Sensing* **2014,** 52, (11), 6964-6971.
39. Zinke, S. A simplified high and near-constant contrast approach for the display of VIIRS day/night band imagery. *Int J Remote Sens* **2017,** 38, (19), 5374-5387.
40. Miller, S. D.; Combs, C. L.; Kidder, S. Q.; Lee, T. F. Assessing Moonlight Availability for Nighttime Environmental Applications by Low-Light Visible Polar-Orbiting Satellite Sensors. *J Atmos Ocean Tech* **2012,** 29, (4), 538-557.
41. Miller, S. D.; Turner, R. E. A Dynamic Lunar Spectral Irradiance Data Set for NPOESS/VIIRS Day/Night Band Nighttime Environmental Applications. *Ieee Transactions on Geoscience and Remote Sensing* **2009,** 47, (7), 2316-2329.